Supporting Information

Doping Pt and Strong Metal-Support Interaction as a Strategy for NiMo-based Eletrocatalyst to Boost Hydrogen Evolution Reaction in Alkaline Solution

Jiao Liu,[a,] Zuochao Wang,[a,] Xueke Wu,[a] Dan Zhang,[b] Yan Zhang,[a] Juan Xiong,[a] Zexing Wu,[a] Jianping Lai[a,] and Lei Wang[a,b,]**

[a] Key Laboratory of Eco-Chemical Engineering, Key Laboratory of Optic-electric Sensing and Analytical Chemistry of Life Science, Taishan Scholar Advantage and Characteristic Discipline Team of Eco-Chemical Process and Technology, College of Chemistry and Molecular Engineering, Qingdao University of Science and Technology, Qingdao 266042, P. R. China.

[b] Shandong Engineering Research Center for Marine Environment Corrosion and Safety Protection, College of Environment and Safety Engineering, Qingdao University of Science and Technology, Qingdao 266042, P. R. China

Correspondence and requests for materials should be addressed to J.L. (e-mail: jplai@qust.edu.cn) and L.W. (e-mail: inorchemwl@126.com).

Chemicals: Molybdenumhexacarbonyl ($Mo(CO)_6$, 98%) and deuterium oxide (D_2O) was bought from Sigma-Aldrich. Acetylacetone platinum ($C_{10}H_{14}O_4Pt$, 97%), Acetylacetone palladium ($C_{10}H_{14}O_4Pd$, 34.9%) was purchased from Macklin. Nickel acetate tetrahydrate ($Ni(oAc)_2 \cdot 4H_2O$, 99%) and Triruthenium dodecacarbonyl ($Ru_3(CO)_{12}$, 98%) and Carboxylated multi-walled carbon nanotubes (CNT) was bought from Aladdin.

Preparation of M-Ni_4Mo/CNT: First, 10 mg of processed CNT, 16 mg $Ni(oAc)_2 \cdot 4H_2O$ and 4 mg $Mo(CO)_6$ and 1.1 mg $C_{10}H_{14}O_4Pt$ were mixed and ground in a mortar for 30 minutes to mix evenly. Then, the mixture

was put into a 10 mL quartz bottle and microwaved in a household microwave oven for 60 s. Ru-Ni_4Mo/CNT and Pd-Ni_4Mo/CNT was prepared according to the same experimental procedures except the precious metals used are different.

Preparation of Pt-Ni_4Mo/CNT in different Pt proportions: First, 10 mg of processed CNT, 16 mg $Ni(oAc)_2 \cdot 4H_2O$ and 4 mg $Mo(CO)_6$ and 0.6 mg $C_{10}H_{14}O_4Pt$ (3 wt% Pt-Ni_4Mo/CNT)/1.5 mg $C_{10}H_{14}O_4Pt$ (7 wt% Pt-Ni_4Mo/CNT) were mixed and ground in a mortar for 30 minutes to mix evenly. Then, the mixture was put into a 10 mL quartz bottle and microwaved in a household microwave oven for 60 s.

Characterization. To study the morphology and structure of the catalyst, a scanning electron microscope (SEM) was tested on Hitachi S-4800 instrument. The transmission electron microscope (TEM) and high resolution. TEM (HRTEM) of the catalyst were tested using FEI Tecnai-G2 F30 at an accelerating voltage of 300 KV, and the structure of the catalyst was further characterized. Powder X-ray diffraction (XRD) spectrum recording was performed on an X'Pert-PRO MPD diffractometer, which was run with Cu Kα radiation at 40 KV and 40 mA. The content of elements is determined by inductively coupled plasma atomic emission spectrometer (ICP-AES, Varian 710-ES). X-ray photoelectron spectroscopy (XPS) analysis was performed with an Axis Supra spectrometer using a monochromatic Al Kα source source at 15 mA and 14 kV. Scan analysis with an analysis area of 300 × 700 microns and a pass energy of 100 eV. The spectrum was calibrated by carbon 1s spectrum, and its main line was set to 284.8 eV, and then the valence state of the catalyst was analyzed using Casa XPS software. In situ attenuated total reflection surface-enhanced infrared absorption spectroscopy (ATR-SEIRAS) was utilized to measure the changes of O-H bonding state

of absorbed water molecule. The catalyst that has been tested for stability is scraped from the working electrode by ultrasonic treatment and collected for the next step of SEM, TEM and XRD characterization.

Electrochemical measurements. Disperse 1 mg of the catalyst in 1 mL of a mixed solution of ethanol + 5% Nafion (v: v=1: 0.01), after sonication for 1 h, the different catalysts with the concentration of 1 mg mL^{-1} was obtained. Electrochemical measurements were carried out in a conventional three-electrode battery of a CHI 760E Electrochemical Workstation (Shanghai Chenhua Instrument Corporation, China). A graphite rod electrode was used as the counter electrode, and the reference electrode was a saturated calomel electrode (SCE). All the potentials were calibrated to reversible hydrogen electrode (RHE) according to the Nernst equation: $E_{RHE} = E_{SCE} + 0.0592*pH + 0.2438$. A glassy carbon electrode (GCE, diameter: 3 mm, area: 0.07065 cm^2) was used as the working electrode. Take 10 μL of the mixed slurry and drop it evenly on the surface of the GCE. After it is naturally dried, further electrochemical tests are performed. All potentials reported in this work are corrected using reversible hydrogen electrodes (RHE). In a 1.0 M KOH solution saturated with N_2, linear sweep voltammetry (LSV) was used to test and evaluate the HER performance of the catalyst at a sweep rate of 5 mV s^{-1}. All polarization curves were corrected for 95% iR. The durability test was performed 200 hours at an intial potential of -0.87 V vs. RHE in 1.0 M KOH solution using chronoamperometry. In addition, the LSV after 10,000 cycles of CV was measured to further evaluate the stability of the catalyst. Electrochemical impedance spectroscopy (EIS) measurement was performed at a frequency of 0.1 Hz to 100 kHz in a 1.0 M KOH solution saturated with N_2.

Calculation of turnover frequency (TOF). Owing to the bulk nature of the catalysts, we selected an electrochemical method to obtain the TOF values of each sample. Nearly all the surface active sites were assumed to be accessible by the electrolyte, and then the TOF values could be calculated by the following equation:

$$TOF = \frac{I}{2Fn}$$

where I, n, and F are the current during linear sweep measurement, the number of active site number, and the Faraday constant, respectively. The factor 1/2 is because water electrolysis requires two electrons to evolve one hydrogen molecule from two protons. The active site number were determined from the CV curves measured in 1 M PBS electrolyte (pH = 7). Since it is very difficult to assign the observed peaks to a given redox couple, the surface active sites are nearly in linear relationship with the integrated voltammetric charges (cathodic and anodic) over the CV curves. Assuming a one-electron process for both reduction and oxidation, we can evaluate the upper limit of the active site number according to the follow formula:

$$n = \frac{Q_{cv}}{2F}$$

where the Q represent the whole charge of CV curve.

ECSA measurements. To estimate ECSA values of the materials, double-layered capacitance (C_{dl}) was measured using a simple cyclic voltammetry method. Here, the potential window has been chosen to be outside the material's possible faradic region (0.94~1.04 V vs RHE) and CV were recorded at various scan rates ranging from 20-100 mV s^{-1}. The capacitive current density, $\Delta J/2$, was linearly related to scan rate and

the double layer capacitance (C_{dl}) was calculated from the slopes of these straight lines. C_{dl} was further converted into ECSA using the specific capacitance value (~0.04 mF) of a standard 1.0 cm^{-2} surface.

Calculation Setup. We have employed the Vienna Ab Initio Package (VASP) to perform all the density functional theory (DFT) calculations within the generalized gradient approximation (GGA) using the PBE formulation. We have chosen the projected augmented wave (PAW) potentials to describe the ionic cores and take valence electrons into account using a plane wave basis set with a kinetic energy cutoff of 450 eV. Partial occupancies of the Kohn-Sham orbitals were allowed using the Gaussian smearing method and a width of 0.05 eV. The electronic energy was considered self-consistent when the energy change was smaller than 10−5 eV. A geometry optimization was considered convergent when the force change was smaller than 0.03 eV/Å. Grimme's DFT-D3 methodology was used to describe the dispersion interactions. During structural optimizations, the 2×2×1 Monkhorst-Pack k-point grid for Brillouin zone was used for k-point sampling for structures. The free energy (ΔG) for elemental reaction step were calculated as:

$$\Delta G = \Delta E + \Delta EZPE - T\Delta S$$

where ΔE is the difference between the total energy, ΔEZPE and ΔS are the differences in the zero-point energy and the change of entropy, T is the temperature (T =300 K in this work), respectively.

Figures

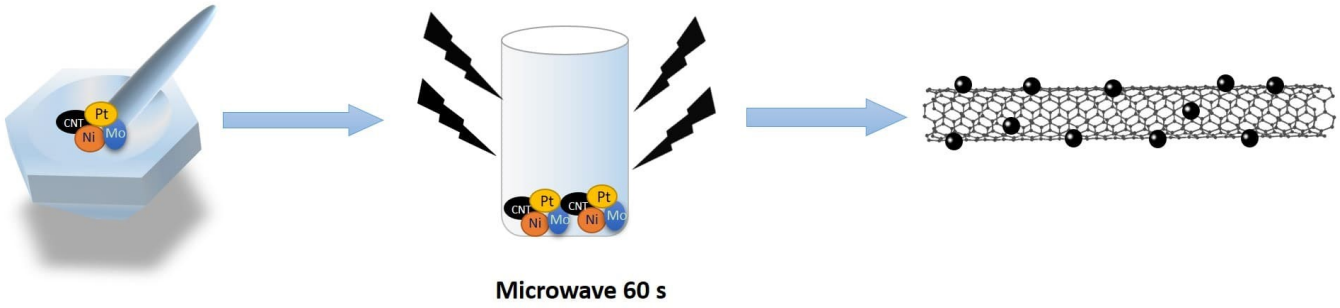

Figure S1. The synthesis diagram of the Pt-Ni_4Mo/CNT nanomaterial.

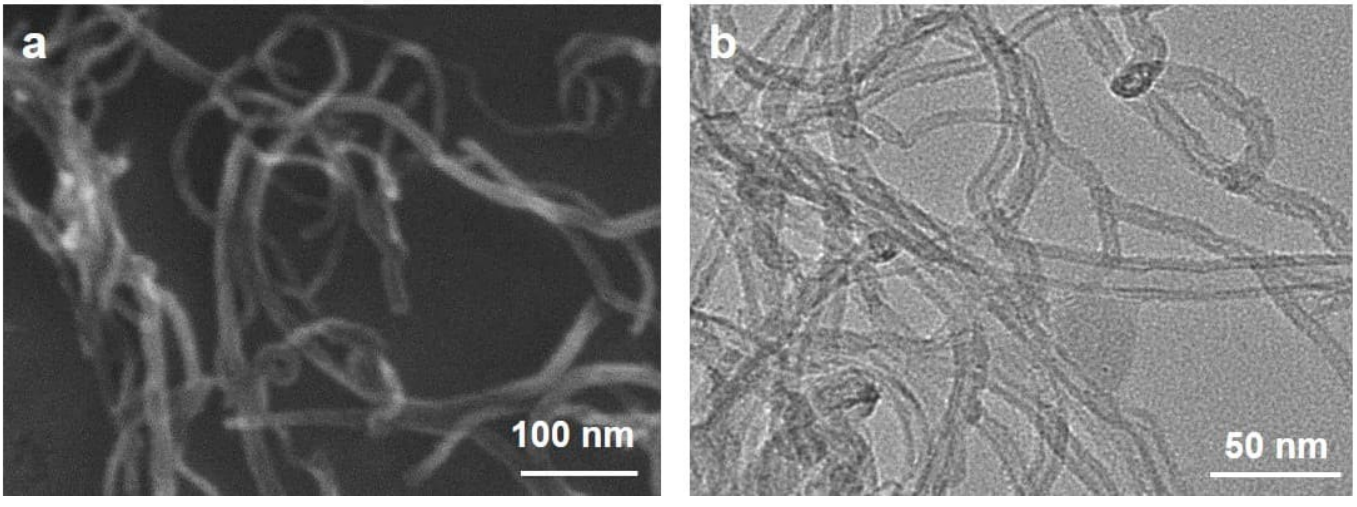

Figure S2. (a) SEM and (b) TEM images of CNT.

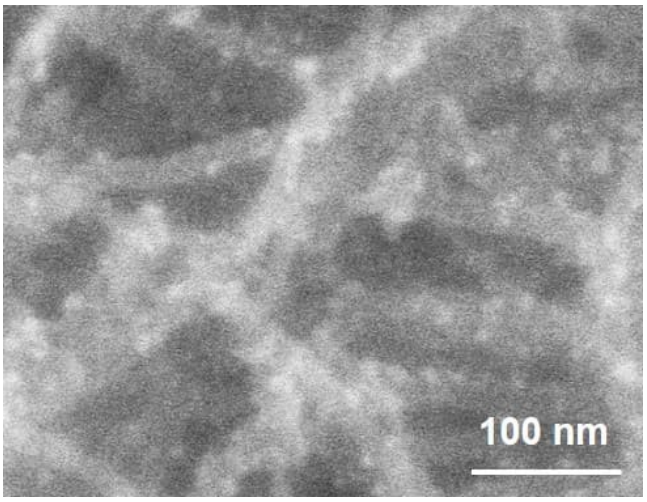

Figure S3. SEM image of Pt-Ni_4Mo/CNT.

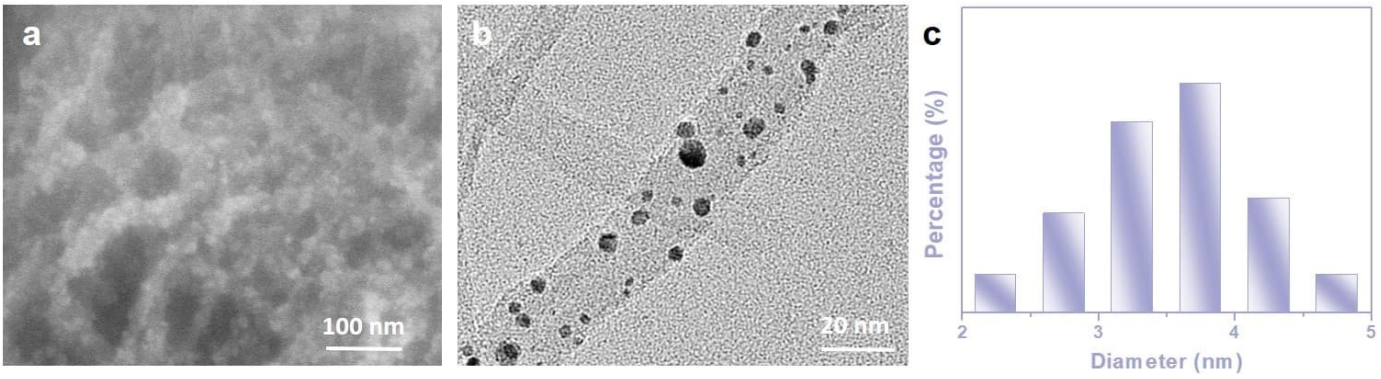

Figure S4. (a) SEM and (b)TEM images of Ni_4Mo/CNT.

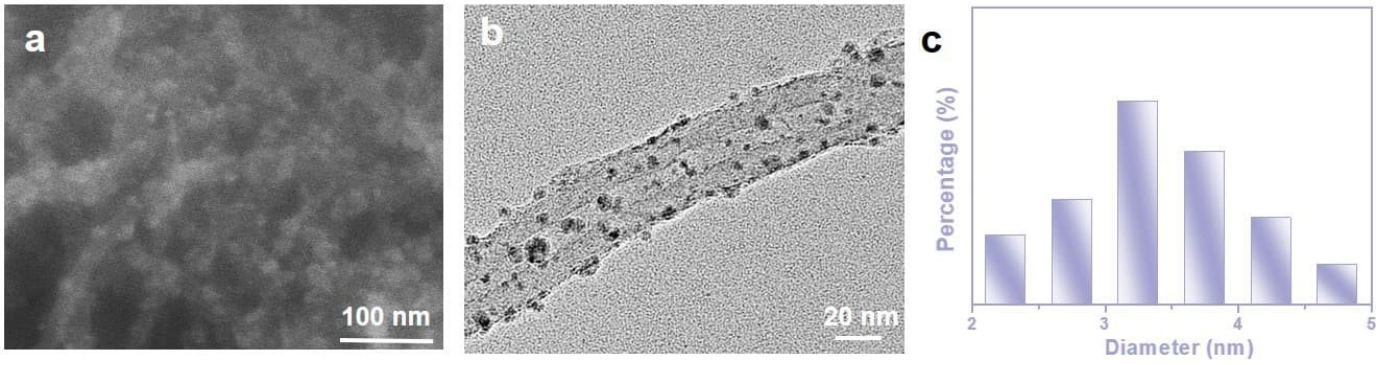

Figure S5. (a) SEM and (b)TEM images of Ru-Ni_4Mo/CNT.

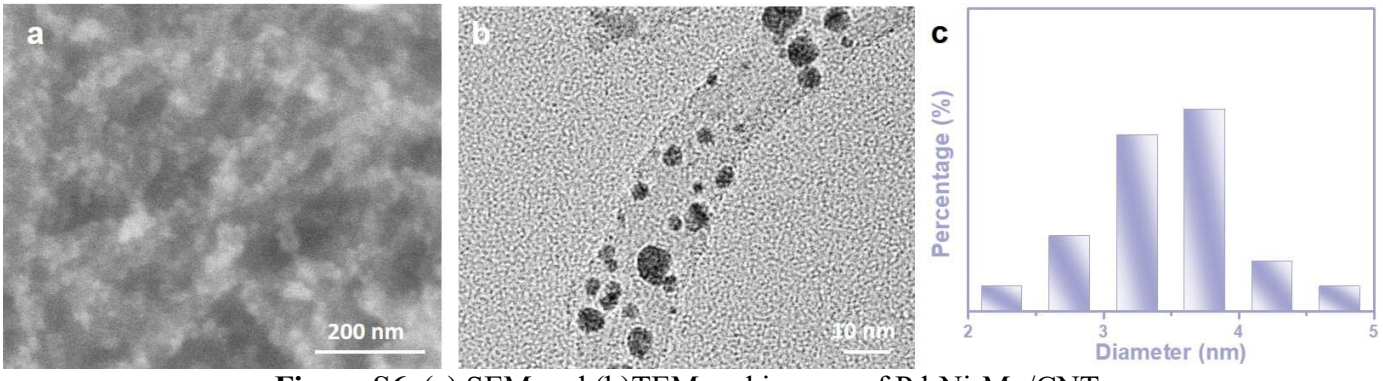

Figure S6. (a) SEM and (b)TEM and images of Pd-Ni_4Mo/CNT.

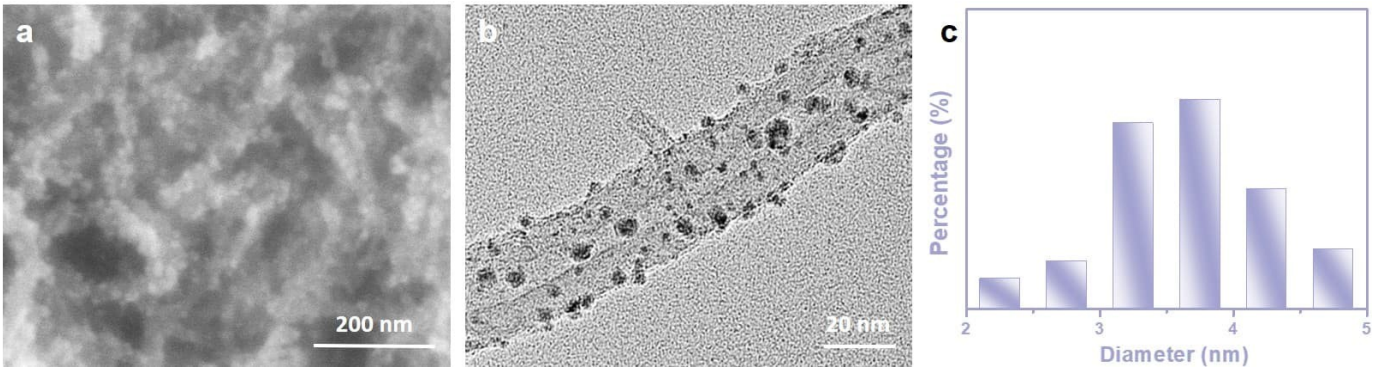

Figure S7. (a) SEM and (b) TEM images of 3 wt% Pt-Ni_4Mo/CNT.

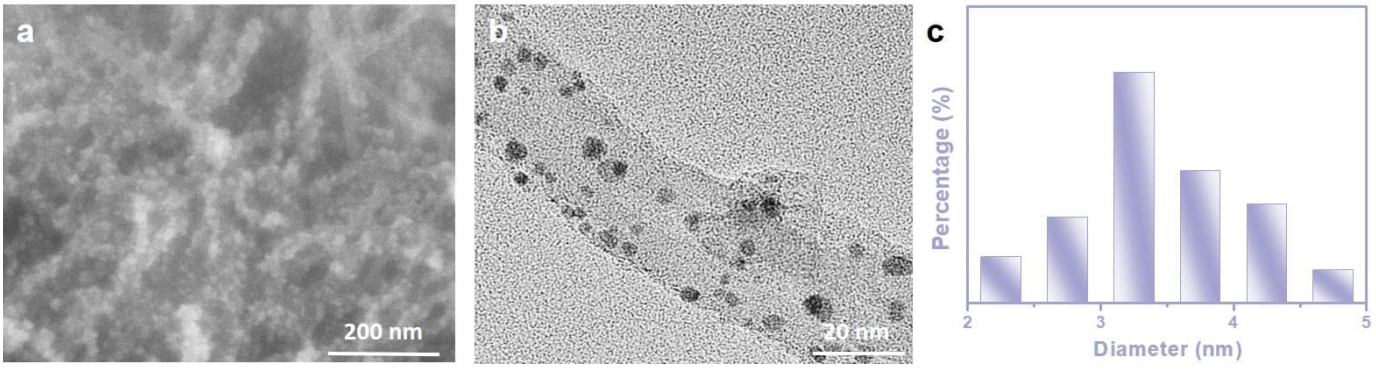

Figure S8. (a) SEM and (b) TEM images of 7 wt% Pt-Ni_4Mo/CNT.

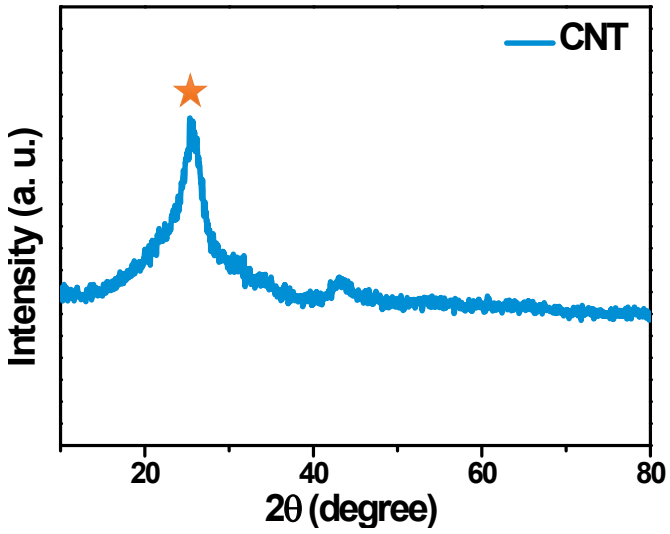

Figure S9. XRD pattern of CNT.

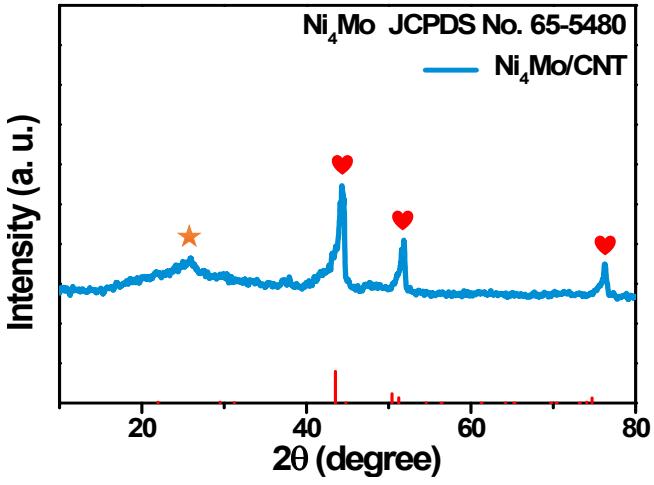

Figure S10. XRD pattern of Ni_4Mo/CNT.

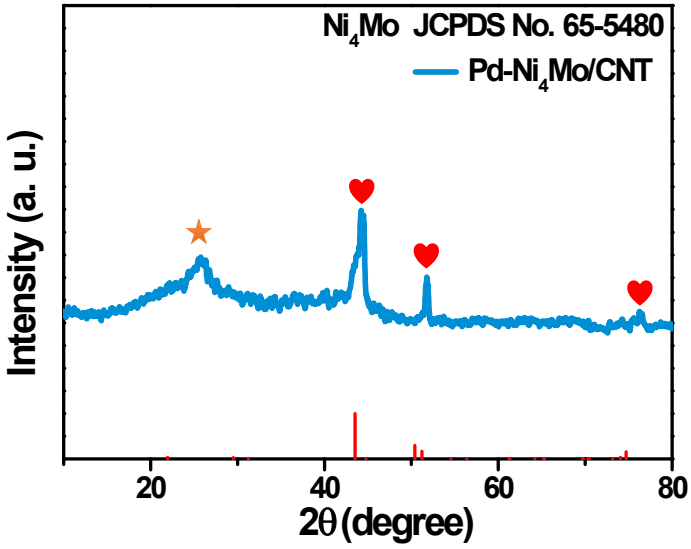

Figure S11. XRD pattern of Pd-Ni_4Mo/CNT.

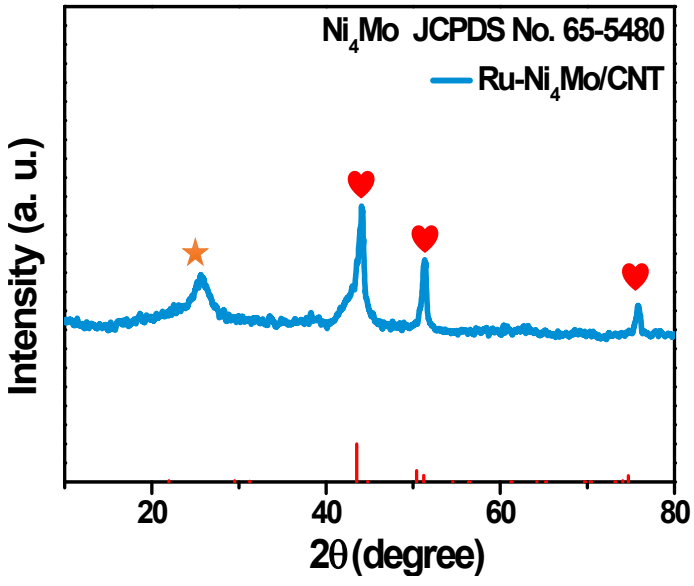

Figure S12. XRD pattern of Ru-Ni_4Mo/CNT.

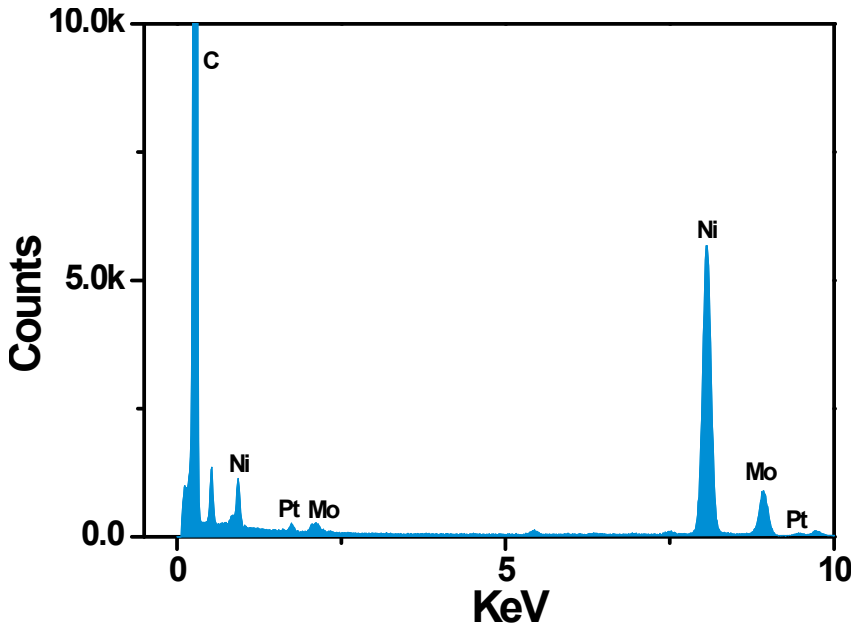

Figure S13. TEM-EDX image for Pt-Ni_4Mo/CNT.

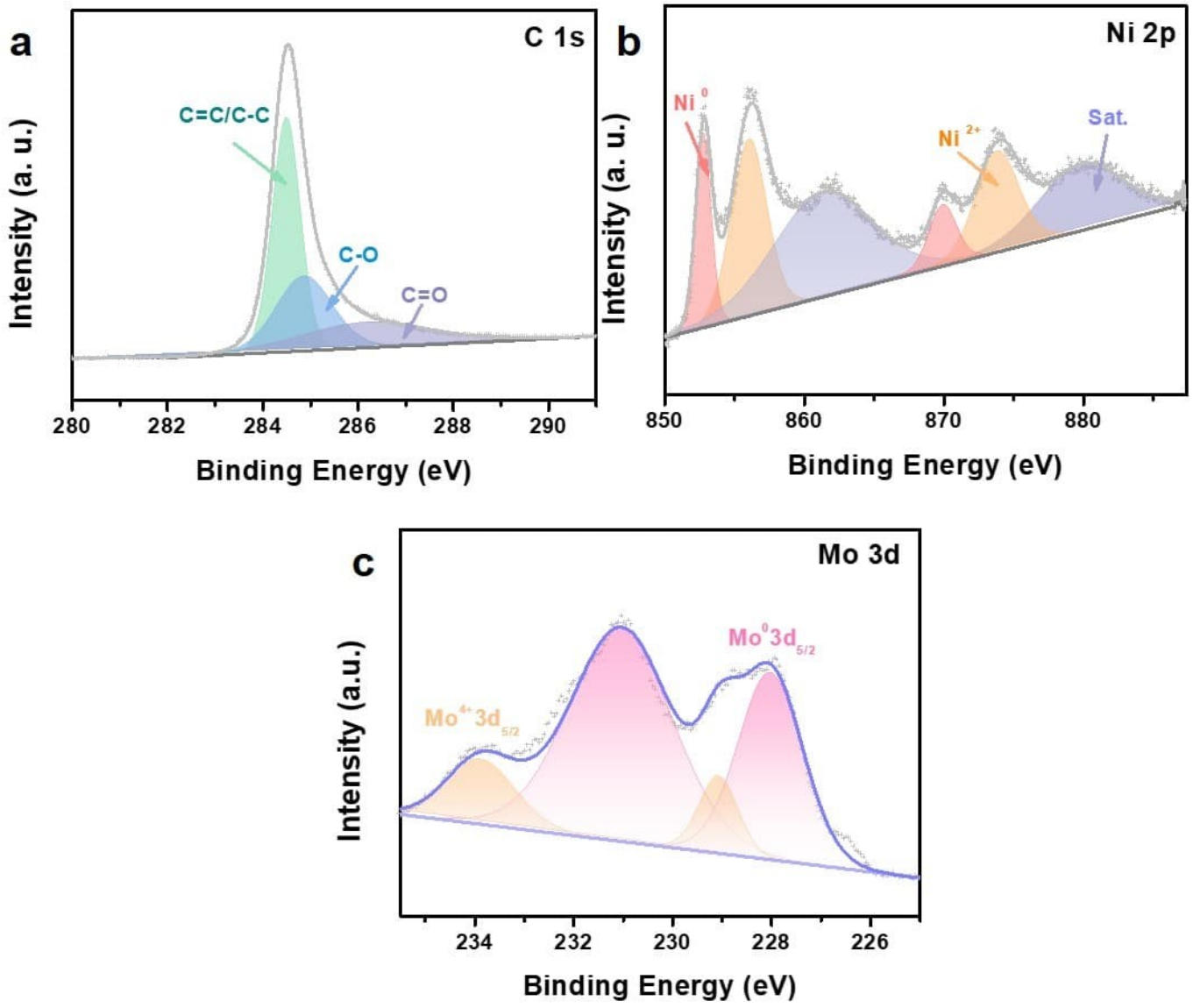

Figure S14. XPS spectra of Ni_4Mo/CNT (a) C 1s, (b) Ni 2p and (c) Mo 3d.

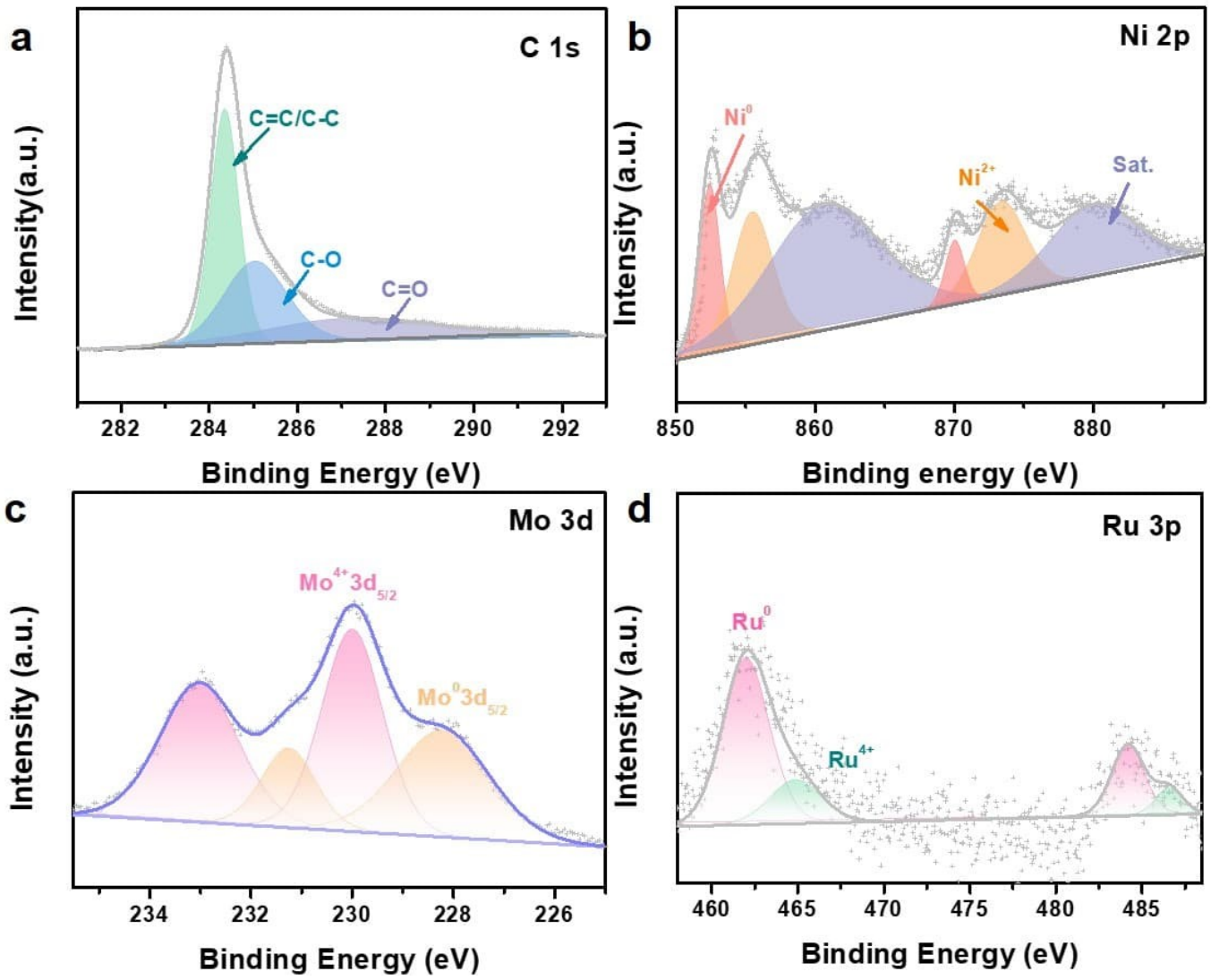

Figure S15. XPS spectra of Ru-Ni_4Mo/CNT (a) C 1s, (b) Ni 2p, (c) Mo 3d and (4) Ru 3p.

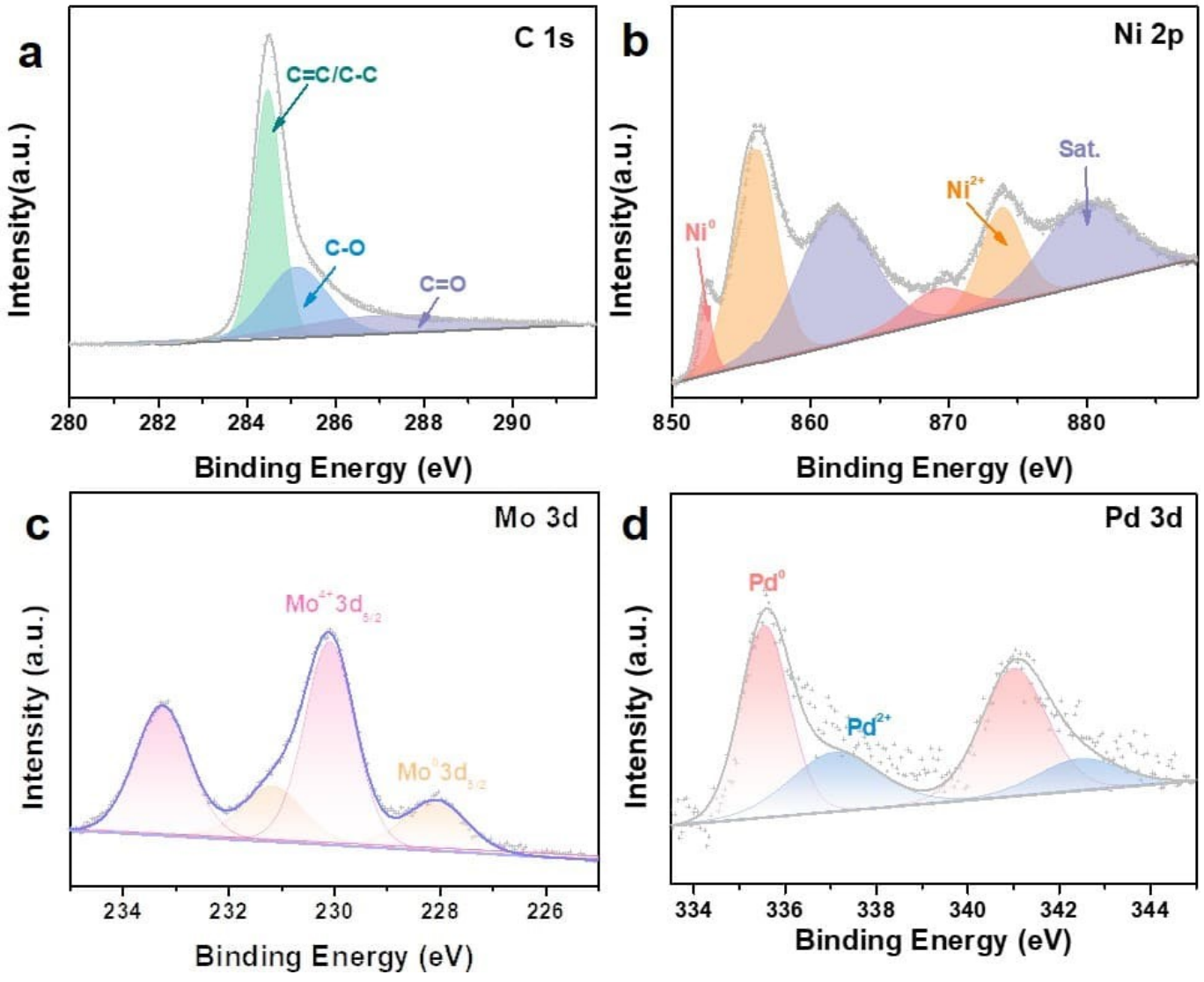

Figure S16. XPS spectra of Pd-Ni_4Mo/CNT (a) C 1s, (b) Ni 2p, (c) Mo 3d and (4) Pd 3d.

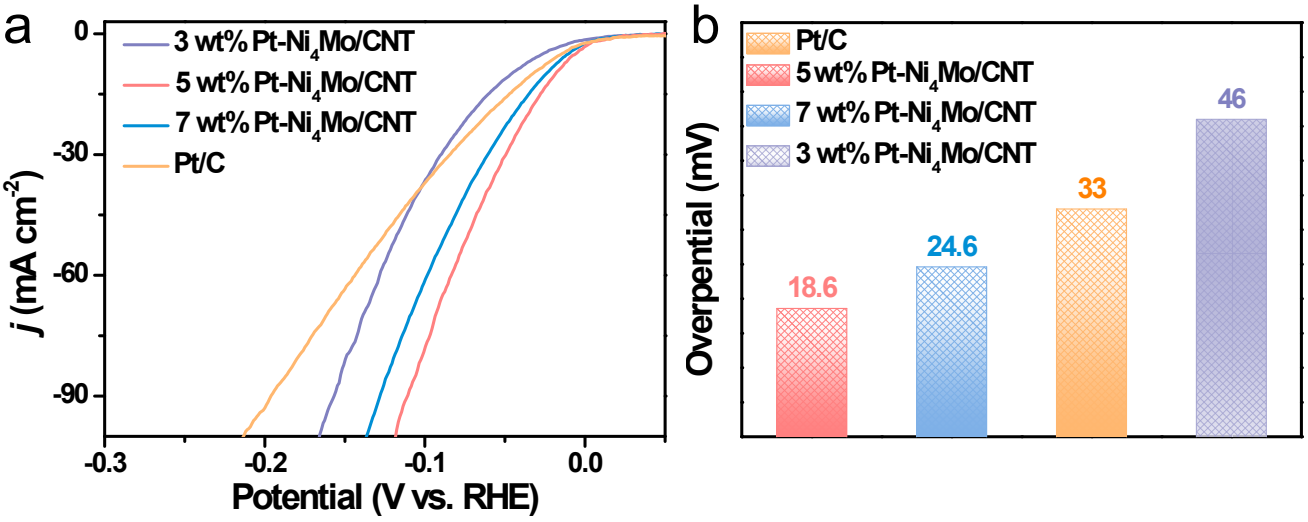

Figure S17. (a) HER polarization curves and (b) the overpotential at 10 mA cm^{-2} of Pt/C, 3 wt% Pt-Ni_4Mo/CNT, 5 wt% Pt-Ni_4Mo/CNT and 7 wt% Pt-Ni_4Mo/CNT.

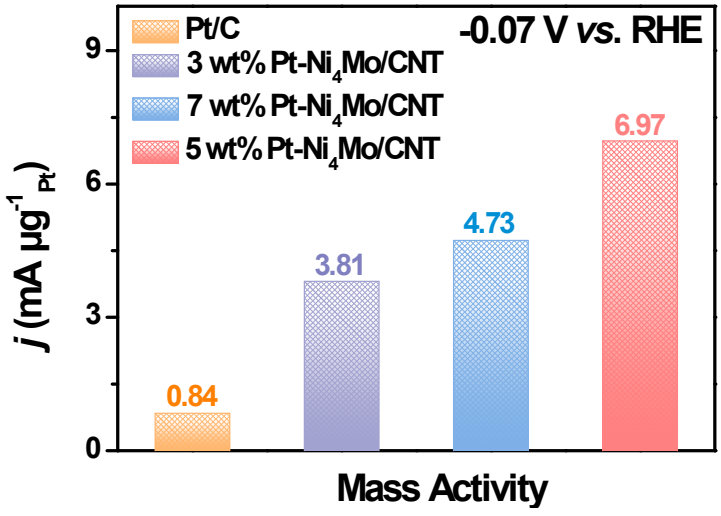

Figure S18. Mass activity at -0.07 V vs. RHE of Pt/C, 3 wt% Pt-Ni_4Mo/CNT, 5 wt% Pt-Ni_4Mo/CNT and 7 wt% Pt-Ni_4Mo/CNT.

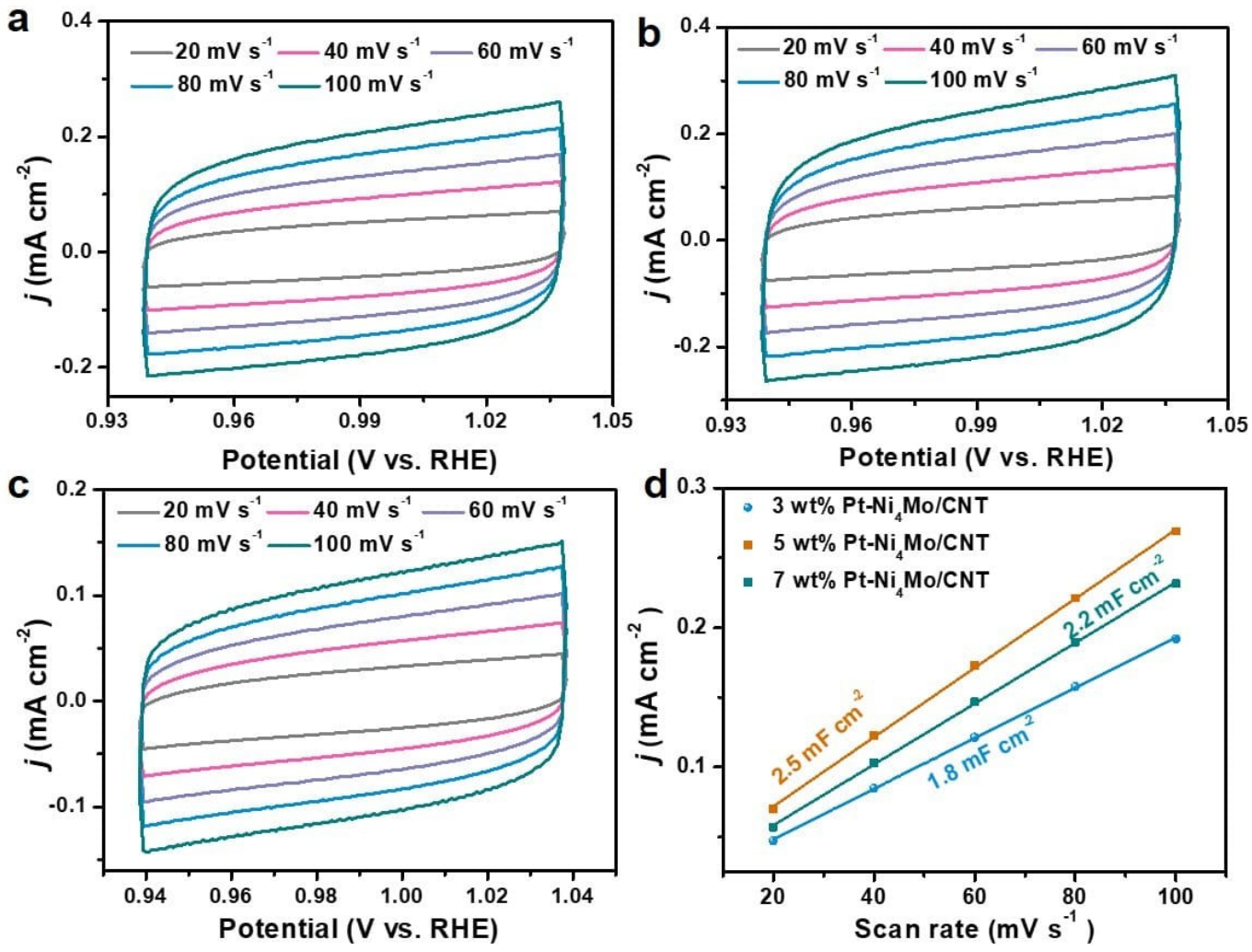

Figure S19. Cyclic voltammograms for (a) 3 wt% Pt-Ni_4Mo/CNT, (b) 5 wt% Pt-Ni_4Mo/CNT, (c) 7 wt% Pt-Ni_4Mo/CNT at scan rates of 20, 40, 60, 80 and 100 mV s^{-1} and (d) Capacitive current at middle potential of CV curves as function of scan rates for 3 wt% Pt-Ni_4Mo/CNT, 5 wt% Pt-Ni_4Mo/CNT, 7 wt% Pt-Ni_4Mo/CNT.

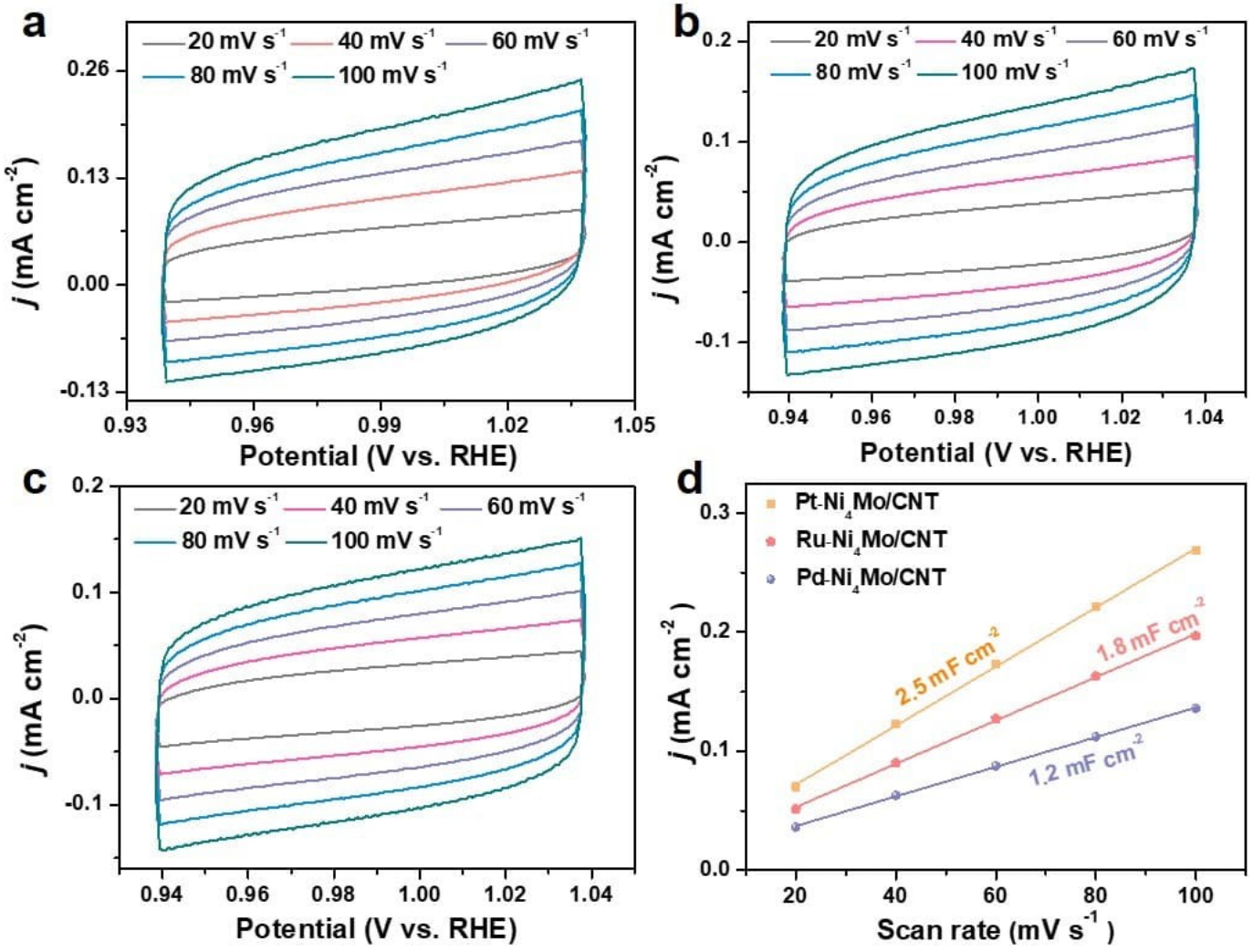

Figure S20. Cyclic voltammograms for (a) Pt-Ni_4Mo/CNT, (b) Ru-Ni_4Mo/CNT, (c) Pd-Ni_4Mo/CNT at scan rates of 20, 40, 60, 80 and 100 mV s^{-1} and (d) Capacitive current at middle potential of CV curves as function of scan rates for Pt-Ni_4Mo/CNT, Ru-Ni_4Mo/CNT, Pd-Ni_4Mo/CNT.

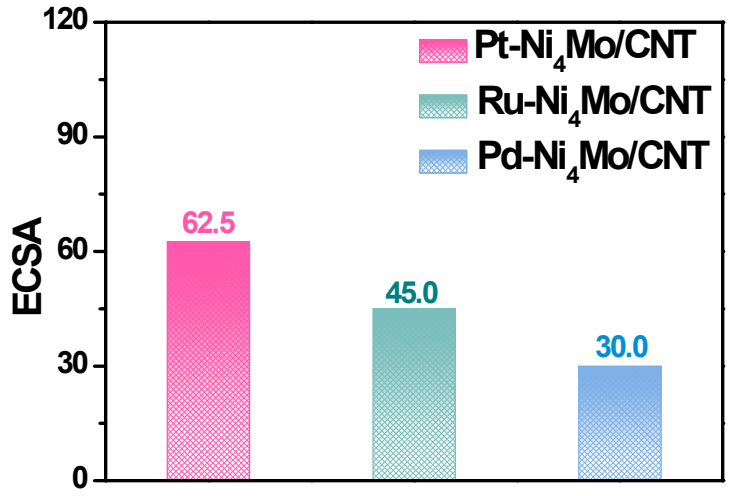

Figure S21. Estimation of the ECSA of Pt-Ni_4Mo/CNT, Ru-Ni_4Mo/CNT, Pd-Ni_4Mo/CNT.

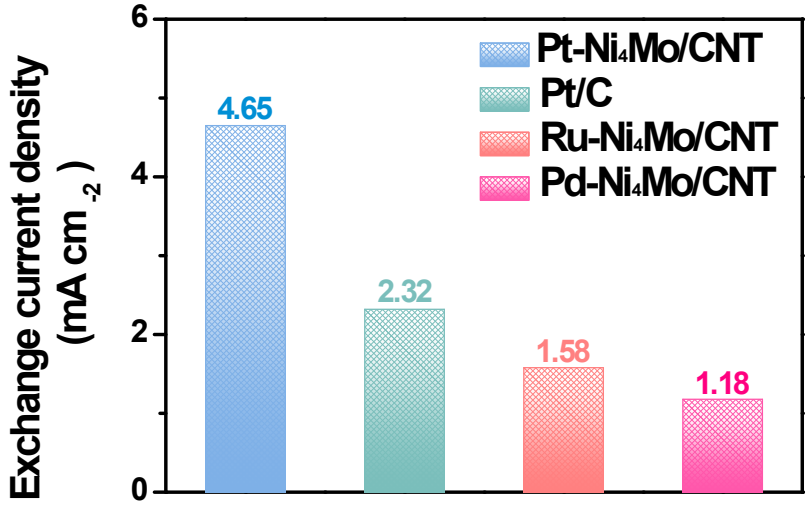

Figure S22. Exchange current dentisy of Pt-Ni_4Mo/CNT, Ru-Ni_4Mo/CNT, Pd-Ni_4Mo/CNT and Pt/C.

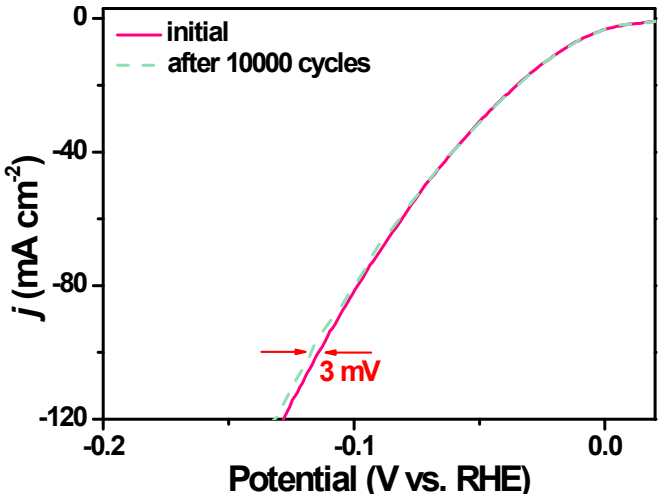

Figure S23. Polarization curves for Pt-Ni_4Mo/CNT catalyst before and after 10000 cycles.

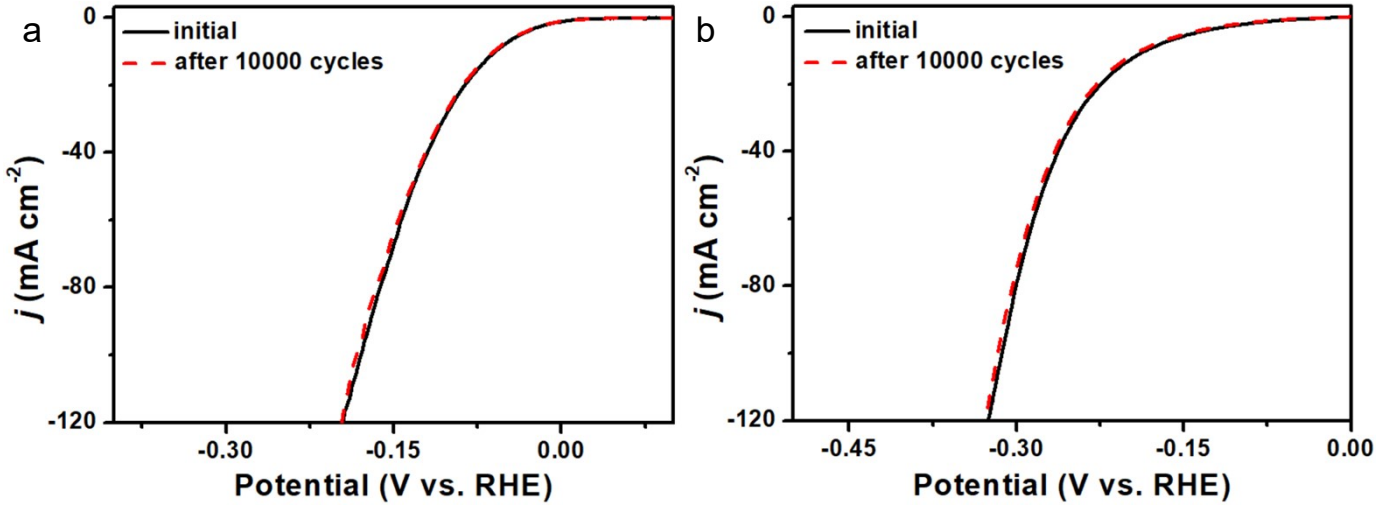

Figure S24. Polarization curves for (a) Ru-Ni_4Mo/CNT and (b) Pd-Ni_4Mo/CNT catalysts before and after 10000 cycles.

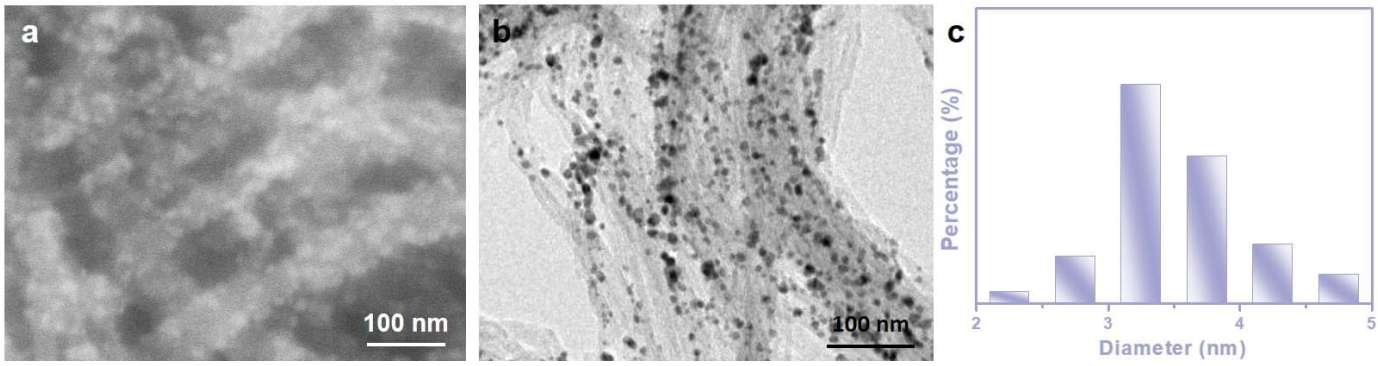

Figure S25. (a) SEM and (b) TEM images of Pt-Ni_4Mo/CNT after stability test.

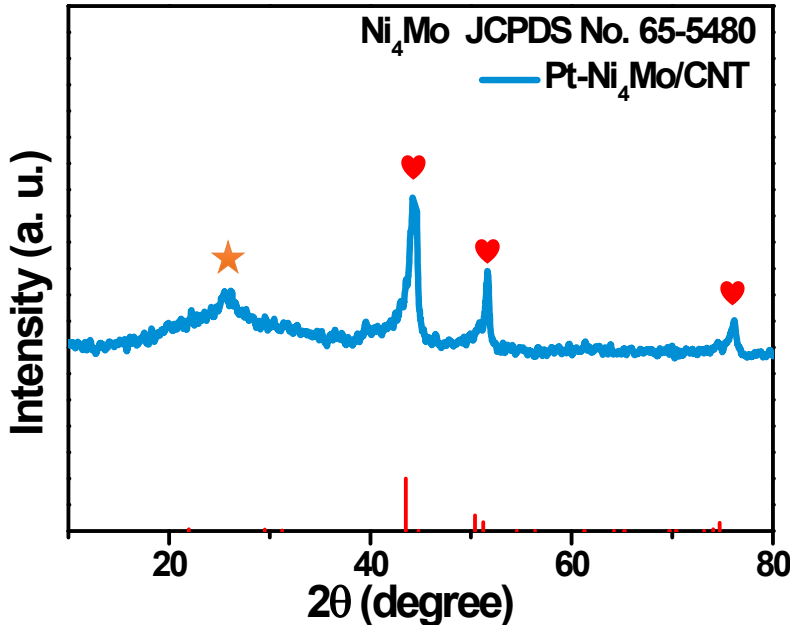

Figure S26. XRD pattern of Pt-Ni_4Mo/CNT after stability test.

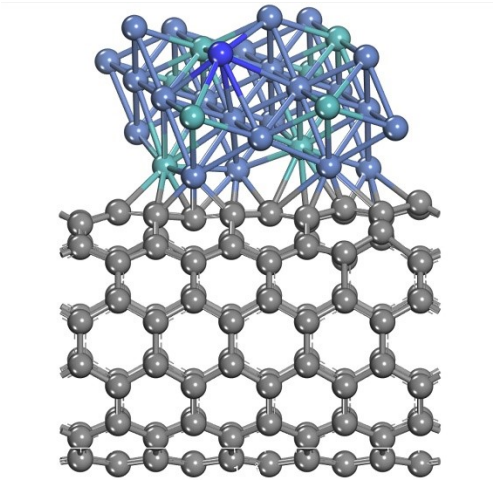

Figure S27. Optimized structures of Pt-Ni_4Mo/CNT.

Table S1. Atomic ratios of Pt-Ni_4Mo/CNT characterized by ICP-AES.

	Ni atom wt%	Mo atom wt%	Noble atom wt%
3 wt% Pt-Ni_4Mo/CNT	78.7	19.2	3.1
5 wt% Pt-Ni_4Mo/CNT	75.9	18.8	5.3
7 wt% Pt-Ni_4Mo/CNT	73.9	18.5	7.6
Ru-Ni_4Mo/CNT	76.0	18.8	5.2
Pd-Ni_4Mo/CNT	75.8	18.9	5.3
5 wt% Pt-Ni_4Mo/CNT after stability test	75.6	19.0	5.4

1

Table S2. Summary of recently reported representative HER catalysts in 1.0 M KOH.

Catalysts	Loading amounts ($\mu g/cm^2$)	η_{10} (mV)	J_{70} (A/mg)	Reference
Pt-Ni_4Mo/CNT	3.47	18.6	6.97	This work
Pt NWs/SL-$Ni(OH)_2$	16.1	70	0.15	*Nat. Commun*. 2015, **6**, 6430
Pt_3Ni_2-NWs-S/C	15.3	42	1.24	*Nat. Commun.* 2017, **8**, 14580
NiO_x/Pt_3Ni Pt_3Ni_3-NWs	15.3	40	2.59	*Angew. Chem. Int. Ed.* 2016, **55**, 12859-12863
A-CoPt-NC	0.419	50	44.9	*Angew. Chem. Int. Ed.* 2019, **58**, 9647-9647
PtNi-O/C	5.1	39.8	7.23	*J. Am. Chem. Soc.* 2018, **140**, 9046-9050
BPed-Pt/GR	14.28	21	5.81	*Angew. Chem. Int. Ed.* 2019, **58**, 19060-19066
Pt/NiO@Ni/NF	92	34	0.532 (at -50 mV)	*ACS Catal.* 2018, **8**, 8866-8872
Pt_{SA}-Ni_3S_2	/	33	/	*Adv. Sci.* 2021, **8**, 2100347
Pt_1/N-C	250	46	/	*Nat. Commun.* 2020, **11**, 1029
Pt-Ni ASs	17	27.7	2.8	*Adv. Mater.* 2018, **30**, 1801741
Ni_3N/Pt	/	50	/	*Adv. Energy Mater.* 2017, **7**, 1601390
N-LDH/2D-Pt	132	31	1.11	*ACS Nano.* 2020, **14**, 10578-10588

Table S3. TOF values of Pt-Ni_4Mo/CNT and reported electrocatalysts in 1.0 M KOH.

Catalyst	Potential (V)	TOF ($_S^{-1}$)	Reference
Pt-Ni_4Mo/CNT	0.1	6.49	This work
Co-NiS_2 NSs	0.1	0.55	*Angew. Chem. Int. Ed.* 2019, **58**, 18676-18682
$CoP/Ni_5P_4/CoP$	0.1	1.22	*Energy Environ. Sci.* 2018,11, 2246-2252
$MoNi_4/MoO_{3-x}$	0.1	1.13	*Adv. Mater.* 2017, **29**, 1703311
P-Fe_3O_4/IF	0.15	0.242	*Adv. Mater.* 2019, **31**, 1905107
NiMoN@NiFeN	0.3	0.09	*Nat. Commun.* 2019, **10**, 5106
Ni-Mo	0.1	0.43	*Small.* 2017, **13**, 1701648
NiMoN/NF-450	0.182	0.5	*J. Mater. Chem. A* 2018,6, 8479-8487
Ni_4Mo/NF	0.087	0.8	*Adv. Mater. Interfaces* 2020, **7**, 1901949
NiS/G-3	0.3	2.475	*Appl. Catal. B Environ.* 2019, 254, 471-478
Mo-doped Ni_2P HNs	0.27	0.125	*J. Mater. Chem. A* 2019,7, 7636-7643
Ni_2P-Ni_3S_2 HNAs/NF	0.1	9.5	*Nano Energy* 2018, **51**, 26-36
Ni_2P/Ni/NF	0.35	0.015	*ACS Catal.* 2016, **6**, 714-721

Table S4. Comparison of the stability of Pt-Ni_4Mo/CNT and reported electrocatalysts in 1.0 M KOH.

Catalyst	η_{10} (mV)	Stability	Reference
Pt-Ni_4Mo/CNT	18.6	200 h @ 100 mA cm^{-2}	This work
Pt_4/Co	6.3	24 h @ 50 mA cm^{-2}	Angew. Chem. Int. Ed. 2021, 60, 25766-25770
WOx-PtNi@Pt DNWs	24	6 h @ 10 mA cm^{-2}	Adv. Energy Mater. 2020, 11, 2003192
Ni_2P–NiP_2 HNPs/NF	59.7	24 h @ 20 mA cm^{-2}	Adv. Mater. 2018, 30, 1803590
N-LDH/2D-Pt	31	50 h @ 10 mA cm^{-2}	ACS Nano, 2020, 14, 10578-10588
Pt_3Ni_2 NWs-S	42	5 h @ 10 mA cm^{-2}	Nat. Commun. 2017, 8, 14580
38 wt% Pt NWs/SL-$Ni(OH)_2$	70	95.7% activity retention after~1 h	Nat. Commun. 2015, 6, 6430.
PtNi-O	39.8	10 h @ 10 mA cm^{-2}	J. Am. Chem. Soc. 2018, 140, 9046-9050
2H/1T-MoS_2	200	200 h @ 150 mV	Nat. Commun. 2019, 10, 1348
Ni_5P_4@$NiCo_2O_4$	27	45 h @ 20 mA cm^{-2}	Adv. Energy Mater. 2018, 8, 1801690
Pt_{SA}–Ni_3S_2@Ag NWs	33	30 h @ 100 mA cm^{-2}	Adv. Sci. 2021, 8, 2100347
Ni@N-CNT/NRs	134	110 h @ 200 mV	Nano Res. 2020, 13, 975-982
Ni/V_2O_3	22	20 h @ 100 mA cm^{-2}	Nano Res. 2020, 13, 2407-2412